The Journal of Physiology

Temporal control of muscle synergies is linked with alpha-band neural drive

Christopher M. Laine[1], Brian A. Cohn[2] and Francisco J. Valero-Cuevas[2,3,4] (iD)

[1]*Chan Division of Occupational Science and Occupational Therapy, University of Southern California, Los Angeles, CA, USA*
[2]*Department of Computer Science, University of Southern California, Los Angeles, CA, USA*
[3]*Department of Biomedical Engineering, University of Southern California, Los Angeles, CA, USA*
[4]*Division of Biokinesiology and Physical Therapy, University of Southern California, Los Angeles, CA, USA*

Edited by: Richard Carson & Mathew Piasecki

Key points

- It is theorized that the nervous system controls groups of muscles together as functional units, or 'synergies', resulting in correlated electromyographic (EMG) signals among muscles. However, such correlation does not necessarily imply group-level neural control.
- Oscillatory synchronization (coherence) among EMG signals implies neural coupling, but it is not clear how this relates to control of muscle synergies.
- EMG was recorded from seven arm muscles of 10 adult participants rotating an upper limb ergometer, and EMG–EMG coherence, EMG amplitude correlations and their relationship with each other were characterized. A novel method to derive multi-muscle synergies from EMG–EMG coherence is presented and these are compared with classically defined synergies.
- Coherent alpha-band (8–16 Hz) drive was strongest among muscles whose gross activity levels are well correlated within a given task.
- The cross-muscle distribution and temporal modulation of coherent alpha-band drive suggests a possible role in the neural coordination/monitoring of synergies.

Abstract   During movement, groups of muscles may be controlled together by the nervous system as an adaptable functional entity, or 'synergy'. The rules governing when (or if) this occurs during voluntary behaviour in humans are not well understood, at least in part because synergies are usually defined by correlated patterns of muscle activity without regard for the underlying structure of their neural control. In this study, we investigated the extent to which comodulation of muscle output (i.e. correlation of electromyographic (EMG) amplitudes) implies that muscles share intermuscular neural input (assessed via EMG–EMG coherence analysis). We first examined this relationship among pairs of upper limb muscles engaged in an arm cycling task. We then applied a novel multidimensional EMG–EMG coherence analysis allowing synergies to be characterized on the basis of shared neural drive. We found that alpha-band coherence (8–16 Hz) is related to the degree to which overall muscle activity levels correlate over time. The extension of this coherence analysis to

Christopher Laine is a research assistant professor in the Chan Division of Occupational Science and Occupational Therapy at the University of Southern California, Los Angeles. He received a BS in Biomedical Engineering and a PhD in Physiological Sciences. His current work utilizes measurements of human brain and muscle activity to study neural control of movement, as well as to develop diagnostics, assessments and rehabilitation strategies.

describe the cross-muscle distribution and temporal modulation of alpha-band drive revealed a close match to the temporal and structural features of traditionally defined muscle synergies. Interestingly, the coherence-derived neural drive was inversely associated with, and preceded, changes in EMG amplitudes by ∼200 ms. Our novel characterization of how alpha-band neural drive is dynamically distributed among muscles is a fundamental step forward in understanding the neural origins and correlates of muscle synergies.

Corresponding author Francisco J. Valero-Cuevas: Department of Biomedical Engineering, University of Southern California, Los Angeles, CA 90089, USA. Email: valero@usc.edu

Introduction

The 'central problem of motor control', as attributed to Bernstein, is the seemingly impossible task of coordinating the many, often redundant, muscles activities that produce movement (Bernstein, 1967). A popular theory is that the nervous system simplifies this task by controlling groups of muscles ('synergies') rather than all muscles individually (Singh *et al.* 2018). While debates persist regarding the neural origins, function, task-specificity and flexibility of muscle synergies (Tresch & Jarc, 2009; Kutch and Valero-Cuevas, 2012; Bizzi and Cheung, 2013; Valero-Cuevas, 2015), their characterization using human electromyographic (EMG) recordings has become an important tool for investigating their relationship to deficits due to injury/disease (Cheung *et al.* 2009, 2012; Gizzi *et al.* 2011; Mileti *et al.* 2020), motor learning (De Marchis *et al.* 2018; Torricelli *et al.* 2020), sports performance (Kristiansen *et al.* 2016; Matsunaga *et al.* 2017) and control of robotic limbs (Alessandro *et al.* 2013; Santello *et al.* 2016).

Common approaches to characterizing synergies identify covariation of gross activity across multiple muscles. However, such covariation may reflect mechanical constraints of a task (Kutch & Valero-Cuevas, 2012), rather than a neural strategy. Intentional synergistic control by the nervous system would imply that coordinated muscles share in common a portion of their neural input. An established technique for identifying shared neural drive is coherence analysis, which quantifies the frequency spectrum of synchronous activity between EMG signals of different muscles. The relevant portion of the surface EMG signal utilized in this method is the timing and density of motor unit action potentials, and thus coherence characterizes the simultaneous reaction of motor neuron pools to simultaneously delivered neural input. It is possible to then probe the origins of that input on a per-frequency basis. Intermuscular coherence >∼6 Hz could not be imposed by simple task mechanics, and distinct frequency bands up to ∼50 Hz have been traced to specific neural origins (Farmer, 1998; Marsden *et al.* 2000; Grosse *et al.* 2002; Grosse and Brown, 2003; Boonstra and Breakspear, 2012; Boonstra, 2013). Under-

standing the neural control of synergies likely requires a combination of both approaches, and would be of benefit for understanding dysfunctional neuromuscular control, e.g. after stroke.

While task requirements (Laine & Valero-Cuevas, 2017) or joint mechanics (Alessandro *et al.* 2020) that impose a high degree of coordination among muscles may favour synergistic control, the relationship between muscle coordination and shared neural drive has not been systematically investigated. Further, ordinary coherence analysis operates on pairs rather than groups of muscles. Accordingly, there is a need to extend current methods that identify shared neural input in a way that allows synergies to be characterized as they are when derived from EMG amplitude covariation.

In this study, we address both of the above limitations. We recorded EMG activity from seven upper limb muscles while participants rotated a crank in the horizontal plane. Because shoulder abduction exacerbates pathological synergies and associated intermuscular coherence after stroke (Ellis *et al.* 2017; Lan *et al.* 2017), participants repeated the task with two levels of shoulder abduction, allowing this interaction, and posture dependence in general, to be explored in non-disabled adults. We first compared pairwise EMG amplitude correlations and coherence within and between shoulder postures. We then used a novel combination of inter-trial coherence and principal component analysis to compare the primary muscle synergy derived from muscle output (EMG amplitudes) with the primary synergy derived entirely from shared neural input (coherence).

We hypothesized a direct relationship between EMG amplitude correlation and intermuscular coherence across pairs of muscles, especially within the alpha (8–16 Hz) band. Coherence in this frequency band is highest in tasks requiring precise muscle coordination (de Vries *et al.* 2016; Laine & Valero-Cuevas, 2017), and is amplified among muscles pathologically coupled after stroke (Lan *et al.* 2017; Chen *et al.* 2018*a*). Extending this logic, we expected that a multi-muscle synergy derived from EMG amplitudes would closely mirror one derived entirely from multi-muscle alpha-band coherence, since this would

occur if these measures characterize different features of the same common neural drive controlling a synergy.

Our results generally support these hypotheses, but also provide evidence that alpha-band coherence may be more related to the monitoring or fine-tuning of synergies as per control requirements of a task, rather than direct muscle activation.

Methods

Ethical approval

All procedures were approved by the University of Southern California internal review board (USC IRB: HS-17-00304) and written consent was obtained from all participants prior to participation. The study conformed to all standards set by the *Declaration of Helsinki*, except for registration in a database.

Study participants

Ten right-handed adults participated in the study (6 males, 4 females, 25–36 years of age), all free from any conditions affecting movement or control of the upper limb.

Task

Participants were seated in front of an unpowered hand ergometer mounted to rotate in the horizontal plane (Fig. 1*A*). The vertical axis of rotation was in line with the right shoulder, the handle set to shoulder height, and distanced such that when the handle was most distant from the participant, the outstretched arm would not hyperextend the elbow or require the participants to lean/rotate their torso. Participants wore a wrist splint and were asked to grip the handle comfortably and rotate the crank without pulling it down. As the crank provided negligible resistance to rotation, activity of the grip and wrist muscles was minimized. This reduced potential variability of shoulder/elbow postures at each phase of rotation, and minimized the potential for widely distributed neural drives, such as are associated with power grips (Baker & Perez, 2017), to influence the upper limb muscles being analysed with respect to their role in crank rotation. Visual feedback of the crank position and a target to follow were provided on a computer screen ∼2 m from the participant, to encourage an even rotation speed (Fig. 1*B*). The crank rotation tasks required a rotation rate of 2 s per full rotation. The participants were then asked to complete 30 clockwise cycles of the crank using each of two shoulder postures throughout the crank rotation (1) with the shoulder abducted (elbow-up) such that the hand, elbow and shoulder moved within one horizontal plane, and (2) with the shoulder adducted (elbow-down) such

that the hand rotated in a plane above the elbow's rotation (Fig. 1*C* and *D*). Practice time was provided prior to each task, with ∼5 min rest periods between tasks. Participants were instructed to use only the arm and to avoid leaning or rotating the torso. We did not physically constrain the torso, both to promote naturalistic upper limb control and because participants had no difficulty restricting torso movement in this task.

Data acquisition

Crank position. The crank angle was sent wirelessly to a PC at 90 Hz using a Vive Tracker (HTC, Taoyuan City, Taiwan). A custom game was designed in C# to collect, record and save the angle data and provide live real time feedback to the user (Unity3D, San Francisco, CA, USA). Custom hardware provided a TTL pulse via an Arduino MEGA (Arduino, Somerville, MA, USA) to synchronize EMG and angle measurements.

EMG recording. We collected EMG signals at 1 kHz from seven muscles of the right upper extremity using a DataLINK system and associated software (Biometrics Ltd, Newport, UK). Surface EMG sensors (Biometrics Ltd SX230: bipolar, gain: 1000, bandwidth: 20–460 Hz) were placed over the short head of the biceps (sbi), the long head of the biceps (lbi), the lateral head of the triceps (tri), the anterior, middle and posterior deltoid (adelt, mdelt and pdelt, respectively), and the upper trapezius (utrap) following standard recommendations (Hermens *et al.* 2000). Electrode placement and signal quality were confirmed using palpation of each muscle and observation of the EMG during voluntary activation. This set of muscles is sufficient for a general analysis of coupling among the shoulder/elbow muscles relevant for our task. We do not attempt to characterize the full dimensionality of the mechanical task faced by the nervous system, as this would require accounting for all muscles and their actions at each joint (Cohn *et al.* 2018).

Signal conditioning and processing

All signals were processed offline using custom MATLAB software (The Math Works, Natick, MA, USA). EMG signals were first high-pass filtered between 250 and 450 Hz using a second order, zero-phase Butterworth filter, then rectified. This high pass filtering procedure has been used both for calculating coherence and predicting muscle force, as it removes motion artifacts, emphasizes the timing and density of motor unit action potentials, and reduces spectral contamination from their shapes (Potvin & Brown, 2004; Boonstra & Breakspear, 2012; Laine and Valero-Cuevas, 2017, 2020). The procedure has been applied here as a precaution to accentuate motor

unit activity rather than as a necessity, and to facilitate comparison with our previous related work (Laine & Valero-Cuevas, 2017, 2020). To obtain a smoothed EMG amplitude time series (gross muscle activity), the filtered, rectified EMG signals were smoothed using a band-pass filter with cutoffs at 0.2 and 5 Hz. The low-pass cutoff smooths the signal while the high-pass cutoff removes

drifts in signal means that are irrelevant to the task. Smoothing of rectified EMG is a standard practice due to the low-pass filtering effects of muscle (Zajac, 1989) and the fact that during a slow movement, small fluctuations in muscle output beyond about 5 Hz mainly reflect task-irrelevant phenomena such as physiological tremor or unfused motor unit twitches (Allum *et al.* 1978).
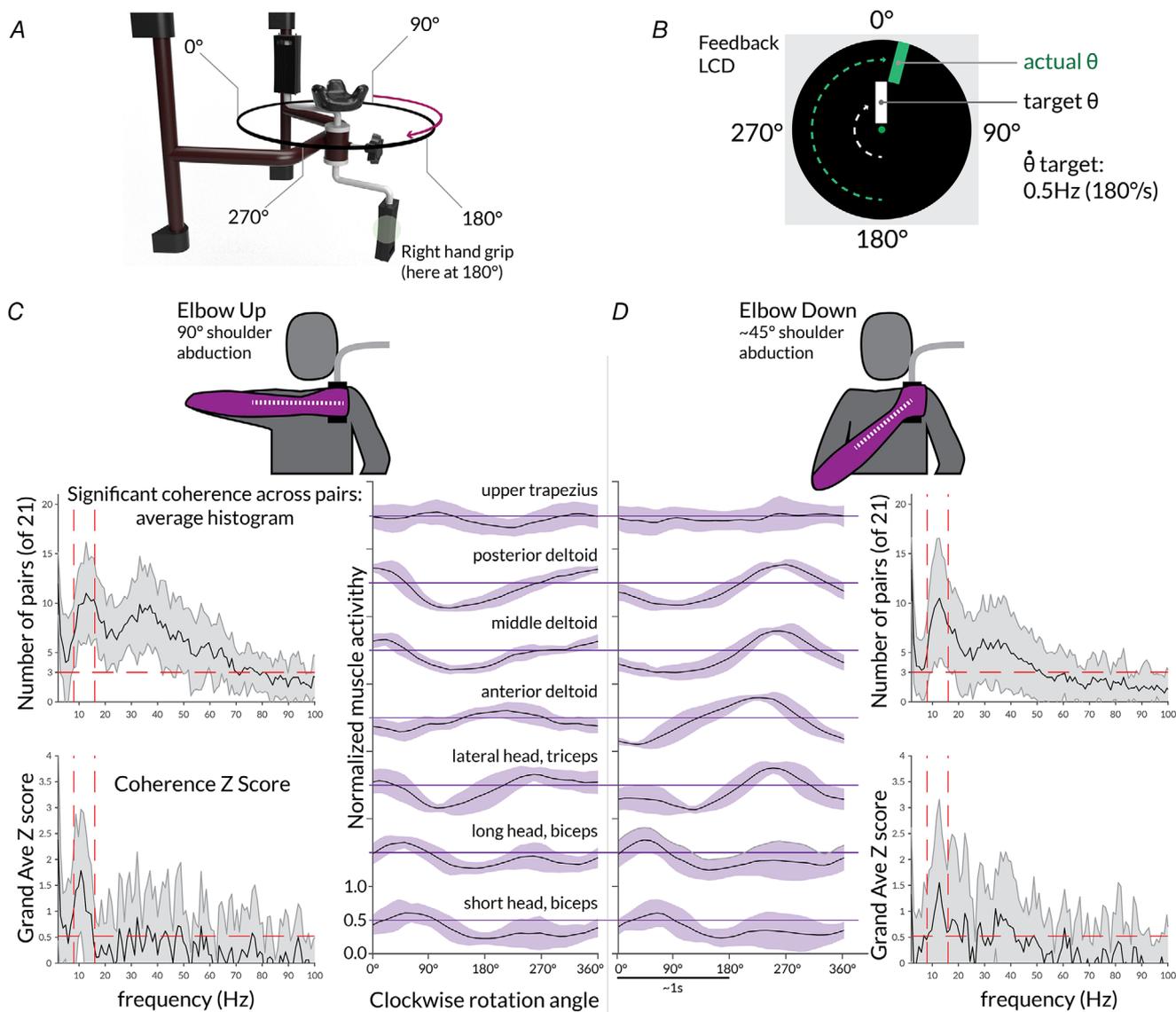
Figure 1. Experimental set-up
A, 10 participants rotated a horizontally mounted upper limb cycle with their right arm in the clockwise direction at a pace of two sec per full rotation. *B*, visual feedback of rotation angle and a target to follow were provided via a computer screen placed in front of the participants. *C* and *D*, surface EMG was collected from 7 muscles of the upper arm as participants completed 30 rotations in each of two shoulder postures: elbow-up, with the shoulder abducted (*C*, time series) and elbow-down (*D*, time series). These time series traces show the mean and standard deviation (shading) for smoothed EMG amplitudes recorded from 10 participants. Units have been normalized to max (1) and min (0) EMG amplitude per cycle prior to averaging. The coherence histograms (*C* and *D*, top) depict the across-participant mean and standard deviation (shading) in the number of muscle pairs showing significant coherence at each frequency. Below each histogram is the mean and standard deviation of coherence magnitudes (*Z*-score), again averaged across the 21 muscle pairs per participant prior to constructing the grand average. [Colour figure can be viewed at wileyonlinelibrary.com]

Statistical procedures

EMG correlations. Per participant, the smoothed EMG amplitudes for each pair of muscles were tested for temporal covariation using Pearson's correlation. Each resulting rho value was then normalized using Fisher's *Z* transform (Fz corr = atanh(rho)) prior to statistical comparisons.

Coherence analysis. To determine if EMG signals showed synchronous oscillatory activity indicative of common neural input, we normalized each rectified EMG signal to unit variance and then calculated the magnitude squared coherence between each pair of muscles using the `mscohere` function in MATLAB, specifying 1 s segments, a Hann window taper and overlap of 50%. To confirm that our focus on the alpha-band was appropriate for our muscles and tasks, we conducted two preliminary analyses. Specifically, we converted raw coherence profiles to standard *Z*-scores (Baker *et al.* 2003; Laine & Valero-Cuevas, 2017) and then calculated, per participant, (1) the number of muscle pairs showing significant coherence (*Z*-score >1.65) at each frequency, and (2) the average coherence *Z*-score for each frequency across all 21 pairs. Grand averages were constructed across these significance histograms and mean coherence profiles (Fig. 1*C* and *D*). Group-level significance thresholds have been added to these plots as a visual aid. Histogram values ≥3 indicate that on average, more pairs showed significant coherence than expected by chance (3 of 21 pairs is more than the 5% chance level, derived from a binomial test). Similarly, an average *Z*-score above 0.52 is unlikely to have occurred by chance, as derived from Stouffer's composite *Z*-score method. An individual raw coherence profile can be seen in Fig. 2*Ab*. The 95% confidence level depicted in the figure was derived as previously described (Kattla & Lowery, 2010).

For our statistical comparisons, for each participant, we determined the maximal coherence in the alpha-band (8–16 Hz) for each pair of muscles, and converted this value to Fisher's *Z* using the formula Fz coh = atanh($\sqrt{coh}$). Fisher's *Z* is the minimal common transform that can be applied to both correlation and coherence data when data lengths are equal, thus minimizing the potential impact of statistical assumptions on assessments of their relationship. While coherence is an extension of Pearson's correlation (Gardner, 1992; Myers *et al.* 2004), there is no mathematical reason to assume that 8–16 Hz coherence should directly scale with time-domain amplitude correlations among different muscle pairs.

Comparison of amplitude correlation and coherence. The above procedure for determining pairwise amplitude correlation and coherence was repeated for the elbow-up and elbow-down postures, as well as their difference, for each participant. For each participant, we then determined if amplitude correlations for the 21 unique pairs of muscles were linearly related to the 21 corresponding coherence values (Fig. 2*B* and *C*). This was accomplished by calculating Pearson's correlation coefficient for muscle pairs within each shoulder posture, as well as for the difference between them. Correlations were considered significant at the two-sided 95% confidence level if the correlation coefficient was ≥0.43, derived from the conversion of correlation (rho) to standard *Z*-scores (i.e. atanh(rho)/$\sqrt{[1/(N-3)]} = Z$, where $N = 21$ pairs, and the significance threshold is $Z = 1.96$). To consider any effects consistent at the group level we required at least three individuals to show significant correlation. The binomial probability of three participants out of 10 showing spuriously significant correlation at the 95% confidence level is 0.012, and thus unlikely.

Time–frequency coherence. To determine how coherence changed across the rotation cycle we converted each rectified EMG signal into a time–frequency representation (i.e. spectrogram) using standard convolution with complex Morlet wavelets. For a given frequency, this wavelet is defined as a Gaussian windowed complex sinusoid with a time duration spanning nine cycles of the given frequency. For each rotation of the crank, the complex time series for each frequency of EMG was divided into 36 10-degree rotation phase bins using the continuous crank angle measurements. Accordingly, for each muscle pair, magnitude-squared coherence could be calculated across the 30 rotations using the time–frequency data associated with each 10-degree phase bin. This is very similar to the event-triggered analyses common in EEG studies (Tallon-Baudry *et al.* 1996; Lachaux *et al.* 1999; Roach and Mathalon, 2008), but rather than calculating coherence over 'trials' at time points relative to a stimulus onset, we calculated coherence over 30 rotations, at each of 36 10-degree rotation phases. In summary, for each participant, we quantified coherence across rotation cycles at each frequency and phase of rotation. This analysis was applied to each muscle pair and shoulder posture.

Projection of coherent neural drive onto individual muscles. To understand the relative distribution of coherent drive to each individual muscle, it was necessary to develop a novel method to project pairwise coherence data back onto each muscle, and thus produce a per-muscle time series for a given frequency band of interest. This procedure is not analogous to a measure of spectral power per muscle, as that would not exclusively reflect the magnitude of shared (phase-locked) neural
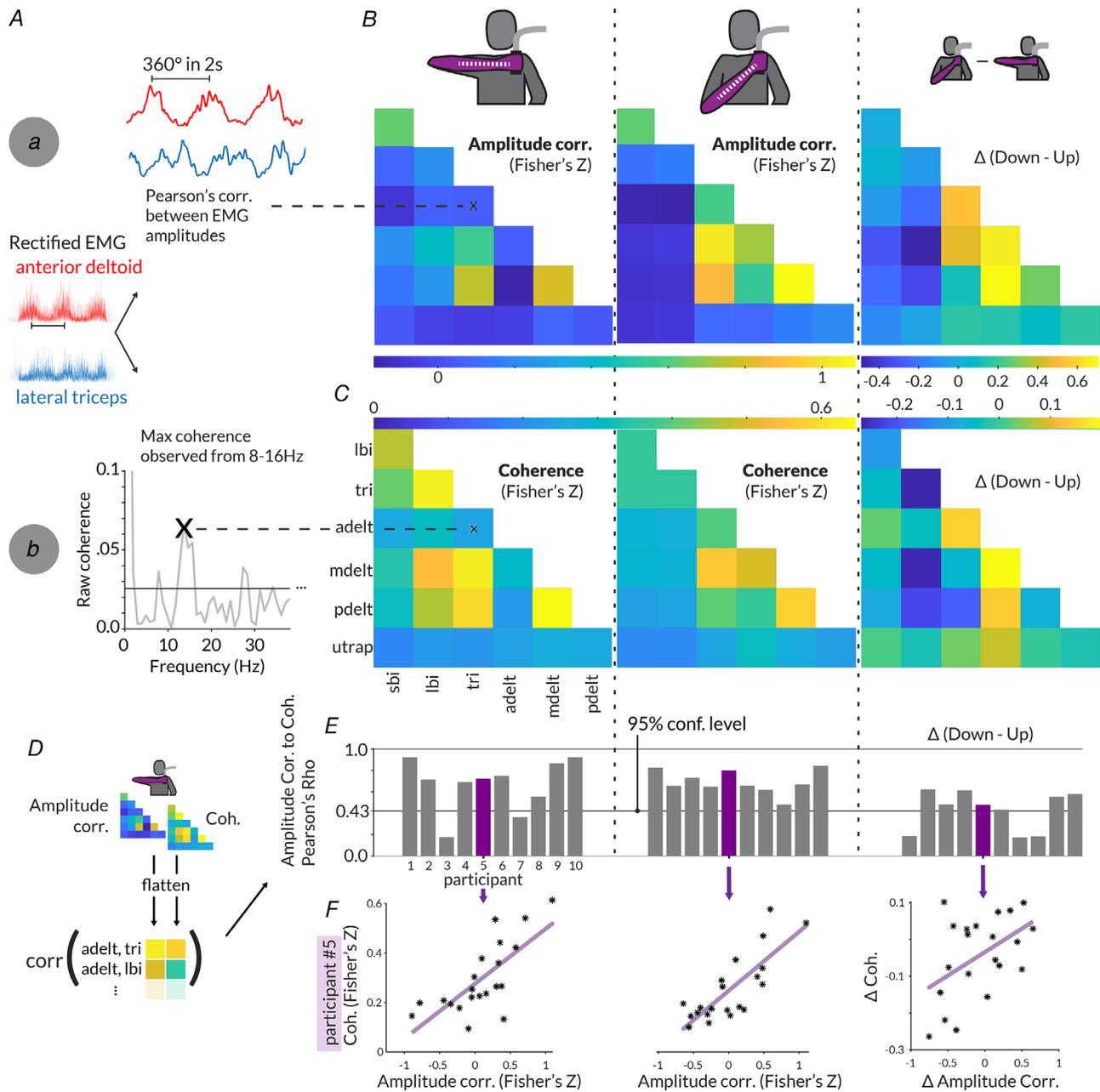
Figure 2. EMG amplitude correlations relate to alpha-band intermuscular coherence
Aa, smoothed, rectified EMG signals for each unique pair of 7 recorded muscles were assessed for temporal correlation by a calculated Pearson's correlation. *B*, average correlations across participants (transformed to Fisher's Z-values) per muscle pair for the elbow-up posture, the elbow-down posture and the difference between the two. The rectified EMG signals were also assessed for coherence (*Ab*) and the largest value between 8 and 16 Hz was recorded for each muscle pair. *C*, average coherence across participants (again transformed to Fisher's Z-values) per muscle pair for each shoulder posture, and the difference between them. Muscle pairs showing high EMG amplitude correlation tended to also show high coherence values. *D*, to determine if a systematic relationship existed between EMG amplitude correlation and alpha-band coherence, Pearson's correlation was calculated across the 21 pairings of 7 muscles, per participant, on EMG amplitude correlation *vs.* the corresponding coherence values. *E*, results of this analysis per participant, and shoulder posture, and for the change in amplitude correlation *vs.* the change in coherence across the two shoulder postures. The horizontal line indicates the 95% confidence level for a correlation (*n* = 21). There was a consistent relationship between EMG amplitudes and coherence across participants for both shoulder postures, as well as for their difference, indicating that while coherence and amplitude correlations were to some extent posture-specific, the relationship between them was relatively stable. *F*, scatterplots showing the relationship between amplitude correlation and coherence for all 21 pairings of the 7 muscles for an example participant. [Colour figure can be viewed at wileyonlinelibrary.com]

drive. In this study, we focus on the alpha-band (8–16 Hz) as it is the strongest and most consistent band of coherence in this task (Fig. 1*C* and *D*), and because previous literature associates this band with task-related muscle coordination requirements (de Vries *et al.* 2016; Laine & Valero-Cuevas, 2017; Reyes *et al.* 2017; Vecchio *et al.* 2019), as well as several clinical conditions which influence muscle coordination and pathological synergies, such as stroke (Dai *et al.* 2017; Lan *et al.* 2017; Chen *et al.* 2018*b*) or Parkinson's disease (Flood *et al.* 2019; Laine & Valero-Cuevas, 2020). For each 10-degree rotation phase bin, we extracted the maximal coherence value in the alpha-band, for each muscle pair (Fig. 3*A*). This allowed us to create, for each 10-degree phase bin, a matrix where each entry corresponds to the max alpha-band coherence for a different muscle pair (Fig. 3*B*). Because magnitude-squared coherence is the frequency-domain expression of a squared Pearson's correlation, taking the square root of each entry in a 7 muscle × 7 muscle coherence matrix produces a

7×7 correlation matrix. Principal component analysis operates on correlation matrices (`pcacov` in MATLAB) by performing singular value decomposition. Thus, performing principal component analysis on our square rooted coherence matrix also allows us to identify its first principal component vector (PC1) of seven 'loadings' that, when squared and multiplied by the total variance explained by PC1, provide an indication of how coherent drive in the 8–16 Hz frequency band was distributed across individual muscles. We repeated this process for each 10-degree phase bin of the rotation cycle to produce a time series of coherent alpha-band drive delivered to each individual muscle (Fig. 3*C* and *D*). It is important to note that this method allows for flexibility with regards to the type of neural drive that is mathematically projected back onto individual muscles. Coherence as derived here represents the strength of phase locking between signals, regardless of any delays between them. But phase information can also be easily obtained from the coherence function itself. For our purposes, we did
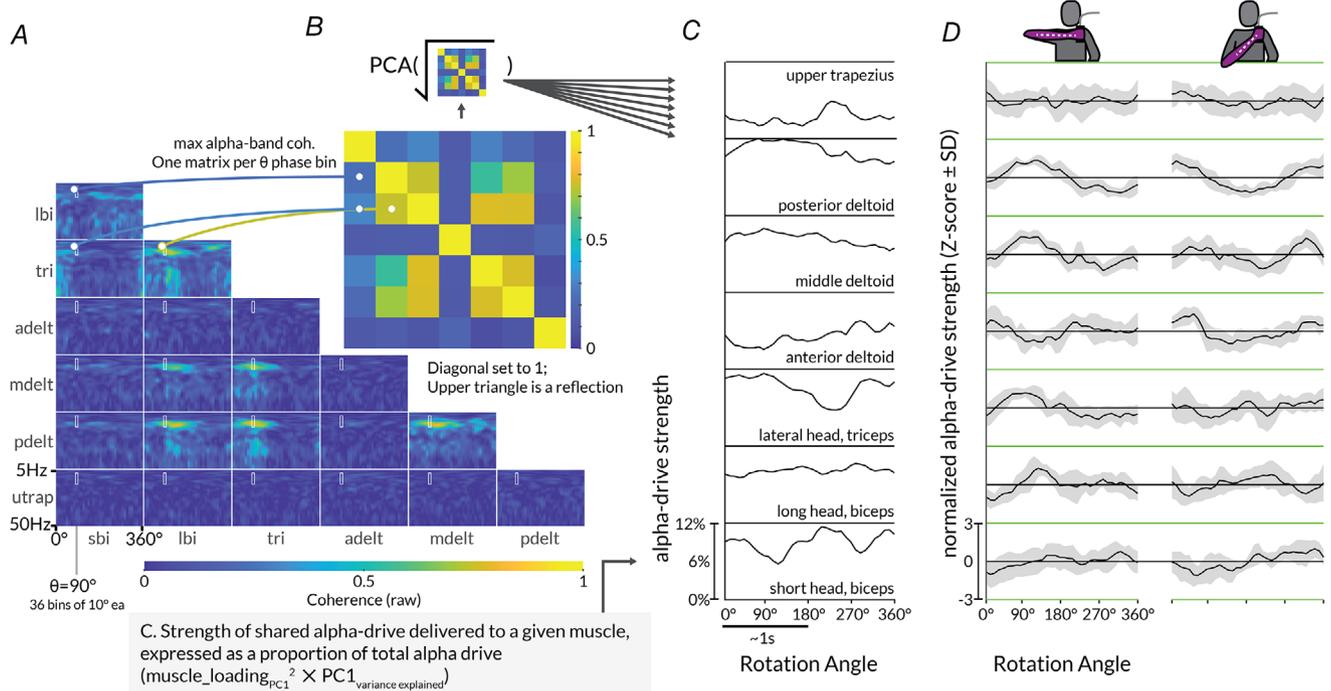
Figure 3. Time–frequency coherence projected onto individual muscles

To evaluate the distribution of coherent neural drive across muscles, and characterize its temporal modulation during the task, we first calculated the cross-rotation coherence between EMG signals in every 10 degree phase of the rotation cycle, forming a time–frequency coherence matrix, as shown for a single participant in *A*. Then, at each phase of the rotation cycle, the maximal coherence value in the 8–16 Hz alpha-band was recorded for each muscle pair. For a given phase of rotation, this resulted in a matrix of maximal coherence values (*B*), which was then subjected to a principal component analysis. This operation produced loadings/weights for each muscle which were used as an index of the strength of intermuscular alpha-band drive to each individual muscle. This was repeated for every phase of the rotation cycle to produce a time series of alpha-band drive for each muscle as shown in *C*. *D*, the average and SD (shading) of the alpha-drive strength for each muscle across the 10 participants. This time series data was then cast in a form comparable with average EMG amplitudes for each phase of the rotation cycle, as shown in Fig. 1. Accordingly, EMG amplitude modulation could be compared directly with the modulation of intermuscular neural drive (Figs 4 and 5) [Colour figure can be viewed at wileyonlinelibrary.com]

not impose a phase constraint on our coherence matrices prior to PCA analysis since it is possible that synergies may be constructed or controlled by a mixture of descending drive and afferent connectivity among muscles. Thus, we chose to examine phase relationships after determining if the strength and intermuscular distribution of coherent 8–16 Hz drive is modulated in a way that indicates synergistic control (see 'Comparison of EMG amplitude and alpha-drive synergies', below). Finally, our method allows for different muscle pairs to be maximally coherent at slightly different frequencies within the alpha-band, and for this possibility to be quantitatively assessed. The choice to use peak frequency adds flexibility and specificity to our analysis, ensures an accurate calculation of phase delays, and is appropriate because coherence profiles have a relatively broad, single peak within the alpha band (e.g. Fig. 1*C* and *D*).

Comparison of EMG amplitude and alpha-drive modulation per muscle. For analysis of EMG amplitude modulation over the course of a rotation cycle, we calculated, per rotation, the average amplitude in every 10-degree phase bin, and then normalized to unit variance. The alpha-band time series data described above were also normalized in the same way prior to further analysis. This allowed us to compare the relative changes in EMG amplitudes along the crank rotation with the relative changes in coherent alpha-band drive delivered to each individual muscle. To determine if temporal modulation of EMG amplitudes was associated with the temporal changes in alpha-band drive (per muscle), we conducted a cross-correlation in which Pearson's rho was calculated after shifting the binned EMG amplitude time series ±10 bins, in 1 bin increments, with respect to the alpha-band time series. Lags were converted to milliseconds (55.5 ms per phase bin) for plotting and interpretation. This was repeated for each muscle and for each individual.

Comparison of EMG amplitude and alpha-drive synergies. To calculate synergies in the traditional way for each individual, the normalized EMG amplitude time series data for all seven muscles was subjected to a principal component analysis. Then, the same normalization and principal component analysis procedure was conducted on the novel per-muscle alpha-band drive time series data. For each individual, we determined the proportion of total variance explained by each principal component for each synergy derivation (EMG amplitude and alpha-band drive), and extracted the squared loadings for PC1. PC1 is the strongest and most unambiguous synergy, which describes a group of temporally co-modulated muscle signals. We then calculated the average of these loadings across participants. To determine if the

average seven-dimensional PC1 loading vector was representative of individual participants, we calculated the cosine similarity between each participant's PC1 loadings and the group average. The mean cosine similarity across participants was tested for statistical significance via comparison to a set of 10,000 surrogate similarities, each calculated after shuffling the PC1 loadings of each participant across muscles. Similar permutation procedures have proven effective in evaluating multi-dimensional relationships across individuals and conditions (Valero-Cuevas *et al.* 2016). To determine if the synergy extracted from EMG amplitudes differed across shoulder postures, we calculated the average cosine similarity between the PC1 loadings derived from each posture, and tested for significance using a permutation test. The same analysis was carried out to examine the effect of shoulder posture on the PC1 loadings derived from alpha-band drive. Finally, we used the same method to determine if the PC1 loadings derived from EMG amplitudes differed from those derived from alpha-band drive within each shoulder posture.

Comparison of EMG amplitude and alpha-drive synergy activation. In addition to determining if the loadings of PC1 were similar across the two synergy derivations (EMG amplitude *vs.* alpha-band drive), we also projected the EMG amplitude and alpha-band drive time series data onto their respective PC1s to derive a 'synergy activation signal', representing modulation of the strength of a given synergy over time. We then cross-correlated the synergy activation signals derived from each method as we had done for individual muscles previously. Finally, to determine the overall time-shift between these activation signals at the group level, we determined the lag at which the correlation between signals was highest in absolute magnitude, and generated a weighted average across the 10 participants. The weights were the absolute correlation coefficients, since a lag has little meaning if signals are not correlated. The entire analysis was repeated for each shoulder posture separately.

Results

EMG amplitude correlation *vs.* coherence

The muscles which showed the largest EMG amplitude correlations among each other were, in general, marked by higher coherence in the 8–16 Hz alpha-band (Fig. 2*E* and *F*). This correlation, calculated across all 21 unique pairs of muscles, was above the 95% confidence level of 0.43 in 8/10 participants for the elbow-up posture, and all participants in the elbow-down posture. As a further confirmation, we also calculated the partial correlation between measures after accounting for the mean coherence between 100 and 300 Hz as a covariate.

Coherence in this range would be elevated by shared noise or shared cross-talk, yet its removal did not eliminate the consistent significant correlation between measures. This procedure would not necessarily remove effects of cross-talk as a source of noise/contamination, but would have eliminated an effect driven by cross-talk.

To further understand the task-specificity of alpha-band coherence and EMG amplitude correlation, we examined the change in each measure between two postures. The change of shoulder posture had different effects across muscle pairs. Many of the largest changes in coherence/correlation involved the anterior and posterior deltoid muscles, as might be expected considering their respective contributions to pushing or pulling mechanically depend on the position of the shoulder. Overall, the posture-induced changes in pairwise EMG amplitude correlations were themselves correlated with the posture-induced changes in coherence across the same muscle pairs (Fig. 2*B*, *C* and *E*, right column). The latter was somewhat variable though, with significant correlation in only 7/10 participants.

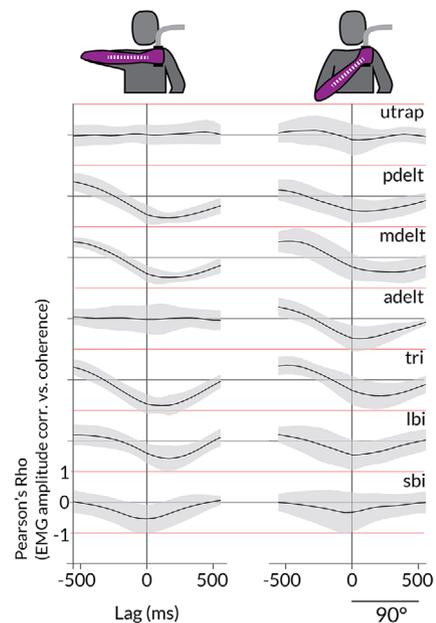### Comodulation of EMG amplitude and alpha-drive per muscle

After statistically distributing pairwise coherence back onto individual muscles (Fig. 3), we cross-correlated the resulting time series for each muscle with the associated EMG amplitude time series for the same muscle (Fig. 4). Some muscles displayed strong correlations between EMG amplitude and alpha-band drive, while others showed no correlation at all for one or both shoulder postures. Interestingly, the strongest correlations were negative, suggesting a delay between modulation of intermuscular alpha-band neural drive and EMG amplitudes. In these cases, intermuscular neural drive preceded EMG amplitude modulations by ~200 ms (negative peaks to the right of 0 lag in Fig. 4).

Synergy identification from EMG amplitudes and coherence

Synergies were identified via principal component analysis of each participant's EMG amplitude data, and their intermuscular alpha-band drive data (Fig. 5*A*). For the elbow-up posture, PC1 derived from EMG amplitudes explained about 60% of the total variance, with the triceps, middle deltoid and posterior deltoid having the highest loadings on average across participants (Fig. 5*B*), with individual participants showing loading profiles very similar to the average across participants (Fig. 5*C*). The same analysis conducted on the coherent alpha-band drive showed again that PC1 explained about half of the total variance, and the associated loadings were consistent

across participants and similar to those derived from EMG amplitudes (Fig. 5*D*). The primary members of this synergy showed the largest alpha-band coherence at ~12 Hz (median (MAD) freq. in Hz: mdelt–pdelt = 12.2 (1.5), mdelt–tri = 11.7 (0.97), tri–pdelt = 12.7 (1.95)). The associated absolute delays at the maximal frequency were, in ms, mdelt–pdelt = 2.9 (1.4), mdelt–tri = 3.3 (1.4) and tri–pdelt = 1.1 (0.21), indicating that these muscles are likely responding to a common ~12 Hz oscillatory drive.

The elbow-down posture also showed high proportions of variance explained by the PC1s of each derivation method, and consistent loadings across individuals; however, the EMG amplitude derived PC1 was similar to that of the elbow-up posture, whereas the PC1 derived from alpha-drive differed from the pattern present in all other conditions. Specifically, the PC1 loadings derived from alpha-band drive in the elbow-down posture did not include the posterior deltoid as a major contributor. The triceps and middle deltoid again showed ~12 Hz maximal alpha-band coherence (11.7 (0.97) Hz) with no appreciable delay (1.8 (0.36) ms), suggesting that the source of alpha-band drive to these muscles is consistent across postures.


Figure 4. Temporal modulation of EMG amplitudes *vs.* alpha-band drive
Average and SD (shading) cross-correlation between EMG amplitude modulation and alpha-band drive strength across phases of the rotation cycle, for each shoulder posture. For most muscles, maximal correlations were negative, and were found at positive lags; changes in alpha-band drive preceded changes in EMG amplitudes for a given muscle. The delay varied across muscles (e.g. adelt), and across postures (e.g. lbi). These results show that intermuscular alpha-band drive is not only temporally modulated across phases of the rotation cycle (Fig. 3), but also that this modulation is time-locked with changes in EMG amplitudes. [Colour figure can be viewed at wileyonlinelibrary.com]

Temporal modulation of synergies derived from EMG amplitudes and coherence

We plotted the projection of EMG amplitude or coherent alpha-band drive onto their respective PC1 axes, yielding a 'synergy activation signal'. The mean and standard deviation of EMG amplitude or alpha-band signals are plotted for each posture in Fig. 6, where it is clear that these signals are largely out of phase, but similar in overall shape. To confirm this, we again
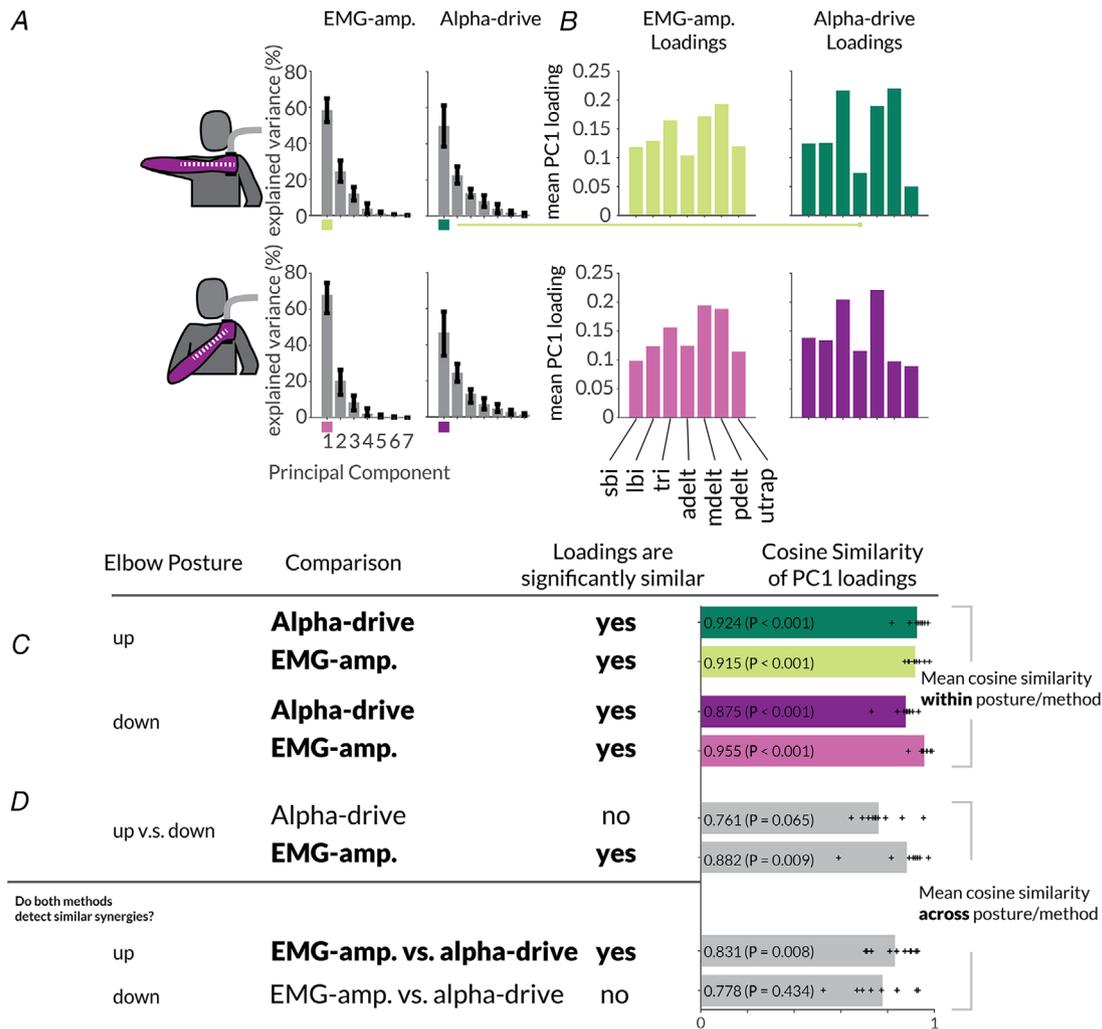
Figure 5. Structure of synergies derived from EMG amplitudes *vs*. alpha-band drive
A principal component analysis was carried out for each participant using (1) the average EMG amplitude time series data for each muscle, and (2) the alpha-band drive time series calculated for each muscle. *A*, scree plots showing the average proportion (across participants) of total variance explained by each principal component for each shoulder posture (elbow-up and elbow-down) and source of synergy derivation (EMG amplitude and alpha-drive). The first component (PC1) explains the majority of the variance in all cases. *B*, relative loadings of PC1 across muscles, averaged across participants. The bar heights represent the fraction of a given muscle's variance that is explained by PC1. The triceps, middle deltoid and posterior deltoid were the most important members of PC1 in nearly all cases. The exception is the loadings of PC1 derived from alpha-drive in the elbow-down posture (bottom right panel), where the posterior deltoid no longer contributes to PC1. *C*, average cosine similarity between each participant's PC1 loadings and the average pattern of loadings displayed in *B*. A high number indicates that the average shown is a faithful representation of individual participant data. The similarity of each participant to the mean is marked with a '+'. The *P*-values signify the statistical probability that the mean cosine similarity could have been observed by chance. In all cases, a consistent pattern of PC1 loadings was observed across participants. *D*, cross-subject average cosine similarity of the PC1 loadings between shoulder postures (elbow-up *vs*. elbow-down), or derivation methods (EMG amplitude *vs*. alpha-drive). For the elbow-up posture, PC1 loadings derived from alpha-drive were similar to those derived from EMG amplitudes, and this was consistent across participants (each marked with a '+'). The same was not true for the elbow-down posture, where PC1 loadings differed between derivation methods. [Colour figure can be viewed at wileyonlinelibrary.com]

conducted a cross correlation after shifting the EMG amplitude-derived activation signal −500 to 500 ms with respect to the intermuscular alpha-drive signal. Once again, their cross-correlations show these signals to be both negatively correlated in magnitude and shifted in time, with changes in alpha-band drive leading changes in EMG amplitudes by ∼200 ms. To the right of Fig. 6, we plot the minimum (largest negative) correlation coefficient for each participant. The vertical line represents the correlation-weighted average lag, which was 174 ms for the elbow-up posture and 204 ms

for the elbow-down posture. Note that because these correlations were conducted over 36 10-degree phase bins, the threshold for statistical significance is 0.33, indicating that nearly all participants, in both conditions, showed a significant relationship between modulation of an EMG amplitude synergy and modulation of a synergy derived from intermuscular alpha-band drive. Although the lags were often very similar across participants (especially for the elbow-up posture), it is worth noting that they do vary across participants and across postures, and thus the relationship appears not to be obligatory.
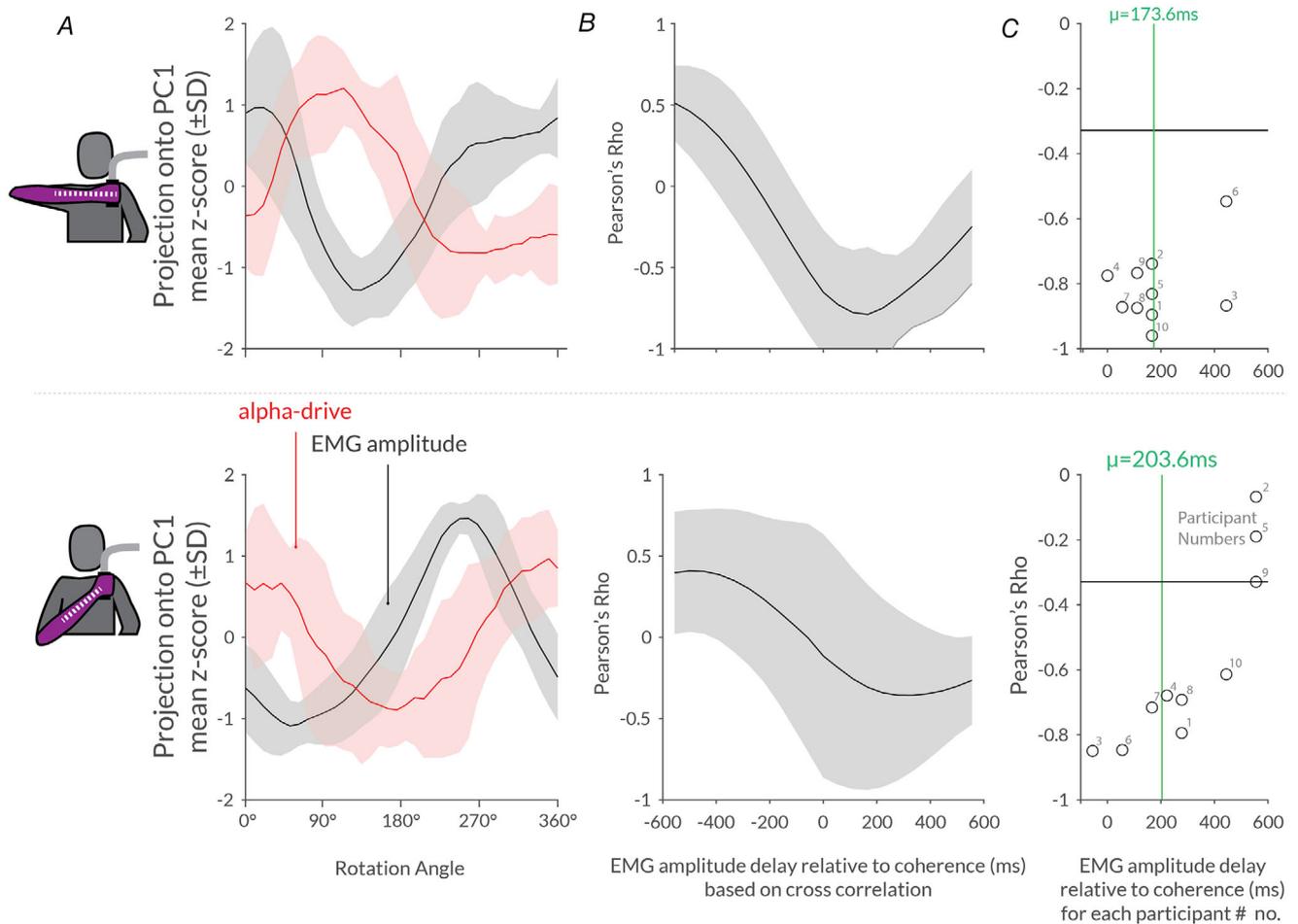
Figure 6. Comparison of synergy activation over time: EMG amplitude *vs*. alpha-band drive
For each individual, the original time series data for EMG amplitudes and alpha-band drive were projected onto their respective first principal components, as characterized in Fig. 5. The average and SD (shading) are shown for each shoulder posture in *A*. The average and SD (shading) cross correlation between the two resulting time series are shown in the lower panel in *B*, again indicating that an inverse relationship exists between modulation of EMG amplitudes and alpha-band drive. The largest correlations were found at positive lags, again indicating that changes in alpha-band drive preceded changes in EMG amplitudes. *C*, the strongest correlation and its associated lag per participant (numbered). The vertical line shows the correlation-weighted average lag and the horizontal line shows the 95% confidence level, indicating statistically non-zero correlation for participants showing larger (in this case more negative) values. The results indicate that the intermuscular alpha-band drive targeting a synergy as a whole is temporally paced according to the overall activity level of the same synergy (as defined by EMG amplitudes, see Fig. 5). The delay and sign of the relationship indicate that increases in alpha-band drive precede decreases in EMG amplitudes by about 200 ms in either condition, although this could vary across individuals and conditions, suggesting that the relationship is not obligatory. [Colour figure can be viewed at wileyonlinelibrary.com]

Discussion

The idea that the nervous system may control groups of muscles as functional units has been an influential, and much debated, hypothesis for many years (Tresch & Jarc, 2009; Kutch and Valero-Cuevas, 2012; Bizzi & Cheung, 2013). However, there remains a disconnect between popular methods which characterize synergies based on patterns of muscle co-activation *vs.* methods which could quantify and characterize the delivery of a common neural drive to multiple muscles of a synergy.

Coherence *vs.* EMG amplitude correlation

We tested for a direct relationship between EMG amplitude correlations and common alpha-band drive (as per intermuscular coherence) across seven upper arm muscles in 10 participants. We found that EMG amplitude correlations and alpha-band coherence were consistently and strongly correlated across muscle pairs, for both arm postures. In fact, the posture-induced changes in both measures were correlated with each other, meaning that although both EMG amplitude correlation and alpha-band coherence are posture-specific, the relationship between the two was stable. Our data indicating a direct relationship between coherence and amplitude correlations may explain previous observations that intermuscular coherence between muscles is highest in tasks that require a high degree of task-relevant muscle coordination (Nazarpour *et al.* 2012; de Vries *et al.* 2016; Laine & Valero-Cuevas, 2017; Reyes *et al.* 2017). These previous studies have shown that for a given muscle pair, the strength and frequency spectrum of coherence can be manipulated by task, with the most likely explanation being that different tasks impose different intermuscular coordination requirements. Our current results, however, indicate that even within a task the degree to which a pair of muscles shows correlated EMG amplitudes (across 21 pairs of muscles) is predictive of their average alpha-band coherence over time, even though coherence changes dynamically during task execution. The relationship between coherence and EMG amplitude correlations might be considered as an artifact of cross-talk or an amplitude-dependent signal to noise ratio, if it were not for the fact that coherence at any given moment in time was not predictable from the amplitude of muscle activity at that same time. Rather, coherence between coordinated pairs of muscles increased as their EMG amplitudes decreased; a phenomenon most clearly observed when assessing groups of coordinated muscles (Fig. 6). Moreover, the temporal variation in alpha-band coherence was about 200 ms offset from variation in EMG amplitudes as a result. Cross-talk and signal quality issues would not be expected to produce an artifactual coherence that is delayed like this, or which is most

apparent during periods of decreasing EMG activity. Nor would one predict that such coherence would be stronger on average between deltoid and triceps muscles compared with adjacent heads of the biceps, as we observed.

Synergies of neural input *vs.* synergies of muscle output

We also expected that synergies could be identified on the basis of their shared neural input (coherence) rather than their output (EMG amplitudes). While some have characterized coherence between selected muscles of a synergy (De Marchis *et al.* 2015; Hu *et al.* 2018), it has never been clear if coherence between muscles of a synergy is determined by their membership within it. In the present study, we developed a method that made it possible to define a synergy based on time–frequency representations of coherence between pairs of muscles. This advancement uncovered that (1) temporal modulation of an intermuscular neural drive was consistently time-locked to modulation of a traditional EMG amplitude-defined synergy, and (2) that the distribution of coherent alpha-band drive across muscles can precisely match the weights/loadings of an amplitude-defined synergy, though this was flexible across tasks. Importantly, amplitude correlations and coherence do not yield redundant information. For example, the alpha-band intermuscular neural drive gained strength and peaked at the rotation phases where EMG amplitudes were decreasing. If this inverse relationship were due to signal interference or electrical cross-talk, coherence should have been largest or smallest when EMG amplitudes were smallest or largest, not delayed by ∼200ms as we observed. Therefore, our findings suggest a physiological rather than artifactual relationship, perhaps related to the inhibition, preparation, or monitoring of a synergy rather than its direct activation.

It should be emphasized that our data do not suggest a simple, direct, causal relationship between coherent alpha-band drive and amplitude correlations. A full description of all possible types of hard-wired and task-dependent connectivity among muscles is not feasible at this time; however, the degree of multi-scale network-level connectivity among muscles, even for simple tasks, is likely complex (Boonstra *et al.* 2015, 2019; Kerkman *et al.* 2018, 2020). Even so, the nervous system must still choose to execute certain tasks through either synergistic or individualized control of muscles. Alessandro *et al.* (2020) have recently suggested that the critical factor motivating formation of synergies may be the need to control internal joint mechanics. This claim was supported by especially high EMG amplitude

correlation between vastus lateralis and medialis muscles, whose actions on the patella must be well balanced, and they may even share most of their neural drive (Laine *et al.* 2015). Our present data support a slightly more general view that functionally relevant amplitude correlations are more likely to be enforced through a neural synergy. For example, we found that the posterior deltoid was both correlated and coherent with the middle deltoid, but when the elbow was lowered, the posterior deltoid contributed much less to the alpha-band synergy. When the elbow is raised, posterior deltoid activity participates in shoulder abduction (a function of the middle deltoid), but works against it when the elbow is lowered (Hik & Ackland, 2019). Accordingly, the elbow-up task may have required more cooperation between deltoid muscles. If it is true that synergies derived from shared drive only reflect task-relevant muscle correlations, it would bridge the present work with a parallel line of investigation, where synergies are defined in the context of a system tuned to control only task-relevant variability (Latash *et al.* 2007). It should be noted that the muscles involved in this shoulder-elbow synergy are particularly relevant for the rotation of the crank. In contrast, the trapezius muscle, while active as a postural muscle, does not directly contribute to crank rotation, and shared little or no alpha-band coherence with the other muscles. While it is possible that artifacts like cross-talk might influence the composition of any synergy derived from surface EMG, such a mechanism would not explain our findings regarding the posterior deltoid. Its overall coherence with the middle deltoid was very similar across the two tasks (Fig. 2*C*), and the ~12 ms delay between signals seems unlikely if coherence just reflected the measurement of one signal from two sensors.

Potential origins and clinical correlates of intermuscular alpha-band drive

Stroke can often cause abnormal coupling and coactivation of elbow and shoulder muscles (Dewald *et al.* 1995), severely restricting upper limb activities. It has been suggested that damaged corticospinal pathways are maladaptively replaced by reticulospinal pathways through changes in the pontomedullary reticular formation and/or ipsilesional cortical control over it (Schwerin *et al.* 2008; Owen *et al.* 2017; McPherson *et al.* 2018; Li *et al.* 2019). Stimulation of the reticulospinal tract through acoustic startle produces a coherent alpha-band drive to the neck and upper limb muscles (Grosse & Brown, 2003), and after stroke, spastic muscles receive (Dai *et al.* 2017) and share (Lan *et al.* 2017; Chen *et al.* 2018*b*) an amplified neural drive of the same frequency. Our results suggest alpha-band coherence between

elbow and shoulder muscles exists even in non-disabled adults, which could mean that the pathological synergies observed in stroke are amplifications of a natural drive rather than the development of a new pathway to muscles. Further, pathological synergies coupling the elbow and shoulder muscles are made worse by abduction of the shoulder (Lan *et al.* 2014, 2017; Ellis *et al.* 2017). We also observed that coherence between shoulder and elbow muscles was, at least for some muscle pairs, notably stronger when the shoulder was abducted (elbow-up posture). This is, to our knowledge, novel evidence that the effect of shoulder abduction on intermuscular coherence/synergies observed in stroke is mirrored in non-disabled adults, and also suggests a possible reticulospinal route for the observed alpha-band intermuscular neural drive.

Alpha-band coherence between muscles is also amplified in Parkinson's disease during static (Flood *et al.* 2019) and dynamic (Laine & Valero-Cuevas, 2020) tasks, and its magnitude can be altered when a task requires a different pattern of intermuscular coordination (Laine & Valero-Cuevas, 2020). We have argued that this could be a fingerprint of damage to the cerebello-thalamo-cortical circuit, which resonates at alpha-band frequencies and synchronizes with motor output through its projections to the cortex and/or pontomedullary reticular formation (Gross *et al.* 2002; Soteropoulos, 2005; Williams *et al.* 2010). Dysfunction of the cerebello-thalamo-cortical circuit may also generate much of the tremor seen in Parkinson's disease (Lewis *et al.* 2007; O'Callaghan *et al.* 2016; Dirkx *et al.* 2016, 2017; Lefaivre, 2016; Muthuraman *et al.* 2018; Madelein van der Stouwe *et al.* 2020) and even essential tremor (Bareš *et al.* 2012; Buijink *et al.* 2015; Louis 2018). It is also critical for the planning, timing and coordination of multi-muscle activities (Diedrichsen *et al.* 2007; Manto *et al.* 2012; Bodranghien *et al.* 2016; Nashef *et al.* 2018, 2019) and perhaps unsurprisingly, its altered function in Parkinson's disease influences muscle synergies (Mileti *et al.* 2020).

It is worth noting that the cerebellum's role in controlling muscle synergies might not be to activate the agonists but instead to activate antagonists which slow or stop a movement, or to dynamically regulate stretch reflex gains associated with a movement (Schieber & Thach, 1985; Thach *et al.* 1993). If the alpha-band drive identified in the present study does reflect a cerebellar circuit operation, it would likely serve these functions, since its magnitude was modulated out of phase with overall muscle activity, peaking as the synergy became less active.

Finally, coordinated patterns of alpha-band drive to members of a synergy might reflect coordinated afferent feedback. For individual muscles, cycles of excitation around the monosynaptic stretch reflex cause oscillations in the alpha-band (Lippold, 1970; Christakos *et al.* 2006;

Erimaki and Christakos, 2008). However, it is not clear how multiple muscles across the limb would become synchronized with each other in a similar manner. Potentially, spinal interneurons could coordinate afferent feedback across synergist muscles (Hart & Giszter, 2010; Levine *et al.* 2014). Some degree of task-specific processing seems necessary though, as exchange of afferent feedback between shoulder and elbow muscles would not be expected to produce simultaneous (near zero phase lag) oscillations across all muscles of a synergy. In summary, while we can only speculate as to the precise physiological function of coherent alpha-band drive, current evidence suggests it is at least informative of afferent reflex loops, cerebellar circuits, or brainstem output, and may be useful for detecting and assessing alterations of neural activity in conditions such as Parkinson's disease or stroke.

Limitations

Our study focused on the alpha-band but we also observed 30–50 Hz (gamma-band) coherence among muscle pairs, primarily in the elbow-up posture, which occurred simultaneously with the alpha-band signal we have characterized here. A direct analysis is beyond the scope of the present investigation but a gamma-band drive could be generated within the same cerebellar circuit that generates the alpha-band drive to muscles during dynamic actions (Popa *et al.* 2013; Soteropoulos, 2005).

Additionally, we focused on the first principal component of either EMG amplitudes or alpha-band drive because other components contributed little to the overall signal modulation, our task was not designed to be high dimensional, and our recorded muscle set was not sufficiently comprehensive to capture the full dimensionality of the task. Also, the first principal component is the most direct and logical extension of pairwise correlation techniques and therefore most well-suited to our study. That said, our methods could easily be extended to multiple synergies defined by any factorization method of choice. It would be interesting, for example, to determine if synergistic drives related to grip or posture overlap with those that more directly control a task such as crank rotation. Our methods could also be applied, with minimal modification, to the analysis of motor unit activity decomposed from intramuscular or high-density surface EMG electrodes. Direct analysis of motor unit activity would reduce various sources of contamination such as cross-talk, which are more likely to occur in standard surface EMG measurements.

A further limitation is the precision with which coherence can be assigned to a given phase of the rotation cycle. For the frequencies analysed, wavelet widths were always longer in duration than the ∼55 ms on average that it took to rotate the crank 10 degrees. Although we obtain a coherence value per 10 degrees of rotation, coherence values in adjacent phase bins are not totally independent. For the present study, this was not a concern, and our methods are appropriate for slow, evenly paced cyclical tasks. Analysis of faster actions with uneven or uncontrolled cycle-phase durations would also be possible with minor modifications to our techniques. For example, using shorter wavelet widths could increase independence of adjacent phase bins, and a non-uniform speed of task execution within or across cycles could be accounted for by task-appropriate pre-averaging and/or weighting of the time–frequency data in each relevant phase bin prior to calculating coherence across cycles.

It is also relevant to note that our sample size is not sufficient for fully characterizing the variance of our measures across the general population, or for identifying any subgroups that may exist. For example, we have no reason to expect that age or sex are relevant biological variables in the context of this study, but this would need to be confirmed using a much larger sample population. It was not within the scope of this study to provide a normative dataset, but rather to uncover, at least in some individuals, a connection between multi-muscle coordination patterns and the distribution of oscillatory neural drive across muscles, and to describe a novel methodology for accomplishing this task.

While further work is required to extend our findings to more frequencies, synergies, muscles and tasks, our work provides a foundation for such efforts, establishing a novel premise and introducing a new methodological strategy for characterizing synergies of neural origin.

Overall, our study provides evidence for a relationship between EMG amplitude correlation and alpha-band coherence measured across pairs of muscles. Our extension of this concept to groups of muscles rather than pairs, and analysis of how multi-muscle coherence is modulated over time, suggest that coherent alpha-band oscillations may relate to the monitoring or fine-tuning of synergies as per control requirements of a task, and are not likely to reflect an oscillatory component of synergy activation signals. The alpha-band drive, being delayed with respect to muscle activation, points towards a sensory/proprioceptive origin, but elucidation of what, if any, functional role is served through propagation of alpha-drive to active muscles remains an important subject for future investigation. While it is clear that alpha-band drive is ubiquitous, task-dependent and altered by neurological damage/disease, a causal role in any particular aspect of motor control has not been established. With a better understanding of how this signal emerges, it could be possible to use its measurement as an assay or marker for neural circuit integrity, and our study contributes to the body of knowledge required for such efforts.

References

Alessandro C, Barroso FO, Prashara A, Tentler DP, Yeh H-Y & Tresch MC (2020). Coordination amongst quadriceps muscles suggests neural regulation of internal joint stresses, not simplification of task performance. *Proc Natl Acad Sci U S A* **117**, 8135–8142.

Alessandro C, Delis I, Nori F, Panzeri S & Berret B (2013). Muscle synergies in neuroscience and robotics: from input-space to task-space perspectives. *Front Comput Neurosci* **7**, 43.

Allum JH, Dietz V & Freund HJ (1978). Neuronal mechanisms underlying physiological tremor. *J Neurophysiol* **41**, 557–571.

Baker SN & & Perez MA (2017). Reticulospinal contributions to gross hand function after human spinal cord injury. *J Neurosci* **37**, 9778–9784.

Baker SN, Pinches EM & Lemon RN (2003). Synchronization in monkey motor cortex during a precision grip task. II. Effect of oscillatory activity on corticospinal output. *J Neurophysiol* **89**, 1941–1953.

Bareš M, Husárová I & & Lungu OV (2012). Essential tremor, the cerebellum, and motor timing: Towards integrating them into one complex entity. *Tremor Other Hyperkinet Mov* **2**, tre-02-93-653-1.

Bernstein N (1967). *The Co-ordination and Regulation of Movements.* Pergamon Press, Oxford.

Bizzi E & Cheung VCK (2013). The neural origin of muscle synergies. *Front Comput Neurosci* **7**, 51.

Bodranghien F, Bastian A, Casali C, Hallett M, Louis ED, Manto M, Mariën P, Nowak DA, Schmahmann JD, Serrao M, Steiner KM, Strupp M, Tilikete C, Timmann D & van Dun K (2016). Consensus paper: Revisiting the symptoms and signs of cerebellar syndrome. *Cerebellum* **15**, 369–391.

Boonstra TW (2013). The potential of corticomuscular and intermuscular coherence for research on human motor control. *Front Hum Neurosci* **7**, 855.

Boonstra TW & Breakspear M (2012). Neural mechanisms of intermuscular coherence: implications for the rectification of surface electromyography. *J Neurophysiol* **107**, 796–807.

Boonstra TW, Danna-Dos-Santos A, Xie H-B, Roerdink M, Stins JF & Breakspear M (2015). Muscle networks: Connectivity analysis of EMG activity during postural control. *Sci Rep* **5**, 17830.

Boonstra TW, Faes L, Kerkman JN & Marinazzo D (2019). Information decomposition of multichannel EMG to map functional interactions in the distributed motor system. *Neuroimage* **202**, 116093.

Buijink AWG, Broersma M, van der Stouwe AMM, van Wingen GA, Groot PFC, Speelman JD, Maurits NM & van Rootselaar AF (2015). Rhythmic finger tapping reveals cerebellar dysfunction in essential tremor. *Parkinsonism Relat Disord* **21**, 383–388.

Chen X, Xie P, Zhang Y, Chen Y, Cheng S & Zhang L (2018*a*). Abnormal functional corticomuscular coupling after stroke. *Neuroimage Clin* **19**, 147–159.

Chen Y-T, Li S, Magat E, Zhou P & Li S (2018*b*). Motor overflow and spasticity in chronic stroke share a common pathophysiological process: Analysis of within-limb and between-limb EMG-EMG coherence. *Front Neurol* **9**, 795.

Cheung VCK, Piron L, Agostini M, Silvoni S, Turolla A & Bizzi E (2009). Stability of muscle synergies for voluntary actions after cortical stroke in humans. *Proc Natl Acad Sci U S A* **106**, 19563–19568.

Cheung VCK, Turolla A, Agostini M, Silvoni S, Bennis C, Kasi P, Paganoni S, Bonato P & Bizzi E (2012). Muscle synergy patterns as physiological markers of motor cortical damage. *Proc Natl Acad Sci U S A* **109**, 14652–14656.

Christakos CN, Papadimitriou NA & Erimaki S (2006). Parallel neuronal mechanisms underlying physiological force tremor in steady muscle contractions of humans. *J Neurophysiol* **95**, 53–66.

Cohn BA, Szedlák M, Gärtner B & Valero-Cuevas FJ (2018). Feasibility theory reconciles and informs alternative approaches to neuromuscular control. *Front Comput Neurosci* **12**, 62.

Dai C, Suresh NL, Suresh AK, Rymer WZ & Hu X (2017). Altered motor unit discharge coherence in paretic muscles of stroke survivors. *Front Neurol* **8**, 202.

De Marchis C, Di Somma J, Zych M, Conforto S & Severini G (2018). Consistent visuomotor adaptations and generalizations can be achieved through different rotations of robust motor modules. *Sci Rep* **8**, 12657.

De Marchis C, Severini G, Castronovo AM, Schmid M & Conforto S (2015). Intermuscular coherence contributions in synergistic muscles during pedaling. *Exp Brain Res* **233**, 1907–1919.

de Vries IEJ, Daffertshofer A, Stegeman DF & Boonstra TW (2016). Functional connectivity in the neuromuscular system underlying bimanual coordination. *J Neurophysiol* **116**, 2576–2585.

Dewald JPA, Pope PS, Given JD, Buchanan TS & Rymer WZ (1995). Abnormal muscle coactivation patterns during isometric torque generation at the elbow and shoulder in hemiparetic subjects. *Brain* **118**, 495–510.

Diedrichsen J, Criscimagna-Hemminger SE & Shadmehr R (2007). Dissociating timing and coordination as functions of the cerebellum. *J Neurosci* **27**, 6291–6301.

Dirkx MF, den Ouden HE, Aarts E, Timmer MHM, Bloem BR, Toni I & Helmich RC (2017). Dopamine controls Parkinson's tremor by inhibiting the cerebellar thalamus. *Brain* **140**, 721–734.

Dirkx MF, den Ouden HE, Aarts E, Timmer M, Bloem BR, Toni I & Helmich RC (2016). The cerebral network of Parkinson's tremor: An effective connectivity fMRI study. *J Neurosci* **36**, 5362–5372.

Ellis MD, Schut I & Dewald JPA (2017). Flexion synergy overshadows flexor spasticity during reaching in chronic moderate to severe hemiparetic stroke. *Clin Neurophysiol* **128**, 1308–1314.

Erimaki S & Christakos CN (2008). Coherent motor unit rhythms in the 6-10 Hz range during time-varying voluntary muscle contractions: Neural mechanism and relation to rhythmical motor control. *J Neurophysiol* **99**, 473–483.

Farmer SF (1998). Rhythmicity, synchronization and binding in human and primate motor systems. *J Physiol* **509**, 3–14.

Flood MW, Jensen BR, Malling A-S & Lowery MM (2019). Increased EMG intermuscular coherence and reduced signal complexity in Parkinson's disease. *Clin Neurophysiol* **130**, 259–269.

Gardner WA (1992). A unifying view of coherence in signal processing. *Sig Process* **29**, 113–140.

Gizzi L, Nielsen JF, Felici F, Ivanenko YP & Farina D (2011). Impulses of activation but not motor modules are preserved in the locomotion of subacute stroke patients. *J Neurophysiol* **106**, 202–210.

Gross J, Timmermann L, Kujala J, Dirks M, Schmitz F, Salmelin R & Schnitzler A (2002). The neural basis of intermittent motor control in humans. *Proc Natl Acad Sci U S A* **99**, 2299–2302.

Grosse P & Brown P (2003). Acoustic startle evokes bilaterally synchronous oscillatory EMG activity in the healthy human. *J Neurophysiol* **90**, 1654–1661.

Grosse P, Cassidy MJ & Brown P (2002). EEG-EMG, MEG-EMG and EMG-EMG frequency analysis: physiological principles and clinical applications. *Clin Neurophysiol* **113**, 1523–1531.

Hart CB & Giszter SF (2010). A neural basis for motor primitives in the spinal cord. *J Neurosci* **30**, 1322–1336.

Hermens HJ, Freriks B, Disselhorst-Klug C & Rau G (2000). Development of recommendations for SEMG sensors and sensor placement procedures. *J Electromyogr Kinesiol* **10**, 361–374.

Hik F & Ackland DC (2019). The moment arms of the muscles spanning the glenohumeral joint: A systematic review. *J Anat* **234**, 1–15.

Hu G, Yang W, Chen X, Qi W, Li X, Du Y & Xie P (2018). Estimation of time-varying coherence amongst synergistic muscles during wrist movements. *Front Neurosci* **12**, 537.

Kattla S & Lowery MM (2010). Fatigue related changes in electromyographic coherence between synergistic hand muscles. *Exp Brain Res* **202**, 89–99.

Kerkman JN, Bekius A, Boonstra TW, Daffertshofer A & Dominici N (2020). Muscle synergies and coherence networks reflect different modes of coordination during walking. *Front Physiol* **11**, 751.

Kerkman JN, Daffertshofer A, Gollo LL, Breakspear M & Boonstra TW (2018). Network structure of the human musculoskeletal system shapes neural interactions on multiple time scales. *Sci Adv* **4**, eaat0497.

Kristiansen M, Samani A, Madeleine P & Hansen EA (2016). Effects of 5 weeks of bench press training on muscle synergies: A randomized controlled study. *J Strength Cond Res* **30**, 1948–1959.

Kutch JJ & Valero-Cuevas FJ (2012). Challenges and new approaches to proving the existence of muscle synergies of neural origin. *PLoS Comput Biol* **8**, e1002434.

Lachaux JP, Rodriguez E, Martinerie J & Varela FJ (1999). Measuring phase synchrony in brain signals. *Hum Brain Mapp* **8**, 194–208.

Laine CM, Martinez-Valdes E, Falla D, Mayer F & Farina D (2015). Motor neuron pools of synergistic thigh muscles share most of their synaptic input. *J Neurosci* **35**, 12207–12216.

Laine CM & Valero-Cuevas FJ (2017). Intermuscular coherence reflects functional coordination. *J Neurophysiol* **118**, 1775–1783.

Laine CM & Valero-Cuevas FJ (2020). Parkinson's disease exhibits amplified intermuscular coherence during dynamic voluntary action. *Front Neurol* **11**, 204.

Lan Y, Yao J & Dewald J (2014). Increased shoulder abduction loads decreases volitional finger extension in individuals with chronic stroke: Preliminary findings. *Annu Int Conf IEEE Eng Med Biol Soc* **2014**, 5808–5811.

Lan Y, Yao J & Dewald JPA (2017). Reducing the impact of shoulder abduction loading on the classification of hand opening and grasping in individuals with poststroke flexion synergy. *Front Bioeng Biotechnol* **5**, 39.

Latash ML, Scholz JP & Schöner G (2007). Toward a new theory of motor synergies. *Motor Control* **11**, 276–308.

Lefaivre SC (2016). The contribution of the cerebello-thalamo-cortical circuit to the pathology of non-dopaminergic responsive Parkinson's disease symptoms. MSc Thesis, Wilfrid Laurier University.

Levine AJ, Hinckley CA, Hilde KL, Driscoll SP, Poon TH, Montgomery JM & Pfaff SL (2014). Identification of a cellular node for motor control pathways. *Nat Neurosci* **17**, 586–593.

Lewis MM, Slagle CG, Smith DB, Truong Y, Bai P, McKeown M, Mailman R, Belger A & Huang X (2007). Task specific influences of Parkinson's disease on the striato-thalamo-cortical and cerebello-thalamo-cortical motor circuitries. *Neuroscience* **147**, 224–235.

Li S, Chen Y-T, Francisco GE, Zhou P & Rymer WZ (2019). A unifying pathophysiological account for post-stroke spasticity and disordered motor control. *Front Neurol* **10**, 468.

Lippold OCJ (1970). Oscillation in the stretch reflex arc and the origin of the rhythmical, 8-12 c/s component of physiological tremor. *J Physiol* **206**, 359–382.

Louis ED (2018). Essential tremor then and now: How views of the most common tremor diathesis have changed over time. *Parkinsonism Relat Disord* **46**, S70–S74.

Madelein van der Stouwe AM, Nieuwhof F & Helmich RC (2020). Tremor pathophysiology: Lessons from neuroimaging. *Curr Opin Neurol* **33**, 474–481.

Manto M, Bower JM, Conforto AB, Delgado-García JM, da Guarda SNF, Gerwig M, Habas C, Hagura N, Ivry RB, Mariën P, Molinari M, Naito E, Nowak DA, Taib NOB, Pelisson D, Tesche CD, Tilikete C & Timmann D (2012). Consensus paper: Roles of the cerebellum in motor control – The diversity of ideas on cerebellar involvement in movement. *Cerebellum* **11**, 457–487.

Marsden JF, Werhahn KJ, Ashby P, Rothwell J, Noachtar S & Brown P (2000). Organization of cortical activities related to movement in humans. *J Neurosci* **20**, 2307–2314.

Matsunaga N, Imai A & Kaneoka K (2017). Comparison of muscle synergies before and after 10 minutes of running. *J Phys Ther Sci* **29**, 1242–1246.

McPherson JG, Chen A, Ellis MD, Yao J, Heckman CJ & Dewald JPA (2018). Progressive recruitment of contralesional cortico-reticulospinal pathways drives motor impairment post stroke. *J Physiol* **596**, 1211–1225.

Mileti I, Zampogna A, Santuz A, Asci F, Del Prete Z, Arampatzis A, Palermo E & Suppa A (2020). Muscle synergies in Parkinson's disease. *Sensors* **20**, 3209.

Muthuraman M, Raethjen J, Koirala N, Anwar AR, Mideksa KG, Elble R, Groppa S & Deuschl G (2018). Cerebello-cortical network fingerprints differ between essential, Parkinson's and mimicked tremors. *Brain* **141**, 1770–1781.

Myers LJ, Erim Z & Lowery MM (2004). Time and frequency domain methods for quantifying common modulation of motor unit firing patterns. *J Neuroeng Rehabil* **1**, 2.

Nashef A, Cohen O, Harel R, Israel Z & Prut Y (2019). Reversible block of cerebellar outflow reveals cortical circuitry for motor coordination. *Cell Rep* **27**, 2608–2619.e4.

Nashef A, Cohen O, Israel Z, Harel R & Prut Y (2018). Cerebellar shaping of motor cortical firing is correlated with timing of motor actions. *Cell Rep* **23**, 1275–1285.

Nazarpour K, Barnard A & Jackson A (2012). Flexible cortical control of task-specific muscle synergies. *J Neurosci* **32**, 12349–12360.

O'Callaghan C, Hornberger M, Balsters JH, Halliday GM, Lewis SJG & Shine JM (2016). Cerebellar atrophy in Parkinson's disease and its implication for network connectivity. *Brain* **139**, 845–855.

Owen M, Ingo C & Dewald JPA (2017). Upper extremity motor impairments and microstructural changes in bulbo-spinal pathways in chronic hemiparetic stroke. *Front Neurol* **8**, 257.

Popa D, Spolidoro M, Proville RD, Guyon N, Belliveau L & Léna C (2013). Functional role of the cerebellum in gamma-band synchronization of the sensory and motor cortices. *J Neurosci* **33**, 6552–6556.

Potvin JR & Brown SHM (2004). Less is more: high pass filtering, to remove up to 99% of the surface EMG signal power, improves EMG-based biceps brachii muscle force estimates. *J Electromyogr Kinesiol* **14**, 389–399.

Reyes A, Laine CM, Kutch JJ & Valero-Cuevas FJ (2017). Beta band corticomuscular drive reflects muscle coordination strategies. *Front Comput Neurosci* **11**, 17.

Roach BJ & Mathalon DH (2008). Event-related EEG time-frequency analysis: an overview of measures and an analysis of early gamma band phase locking in schizophrenia. *Schizophr Bull* **34**, 907–926.

Santello M, Bianchi M, Gabiccini M, Ricciardi E, Salvietti G, Prattichizzo D, Ernst M, Moscatelli A, Jorntell H, Kappers AML, Kyriakopoulos K, Schaeffer AA, Castellini C & Bicchi A (2016). Towards a synergy framework across neuroscience and robotics: Lessons learned and open questions. Reply to comments on: "Hand synergies: Integration of robotics and neuroscience for understanding the control of biological and artificial hands". *Phys Life Rev* **17**, 54–60.

Schieber MH & Thach WT (1985). Trained slow tracking. II. Bidirectional discharge patterns of cerebellar nuclear, motor cortex, and spindle afferent neurons. *J Neurophysiol* **54**, 1228–1270.

Schwerin S, Dewald JPA, Haztl M, Jovanovich S, Nickeas M & MacKinnon C (2008). Ipsilateral versus contralateral cortical motor projections to a shoulder adductor in chronic hemiparetic stroke: implications for the expression of arm synergies. *Exp Brain Res* **185**, 509–519.

Singh RE, Iqbal K, White G & Hutchinson TE (2018). A systematic review on muscle synergies: From building blocks of motor behavior to a neurorehabilitation tool. *Appl Bionics Biomech* **2018**, 3615368.

Soteropoulos DS (2005). Cortico-cerebellar coherence during a precision grip task in the monkey. *J Neurophysiol* **95**, 1194–1206.

Tallon-Baudry C, Bertrand O, Delpuech C & Pernier J (1996). Stimulus specificity of phase-locked and non-phase-locked 40 Hz visual responses in human. *J Neurosci* **16**, 4240–4249.

Thach WT, Perry JG, Kane SA & Goodkin HP (1993). Cerebellar nuclei: Rapid alternating movement, motor somatotopy, and a mechanism for the control of muscle synergy. *Rev Neurol* **149**, 607–628.

Torricelli D, De Marchis C, d'Avella A, Tobaruela DN, Barroso FO & Pons JL (2020). Reorganization of muscle coordination underlying motor learning in cycling tasks. *Front Bioeng Biotechnol* **8**, 800.

Tresch MC & Jarc A (2009). The case for and against muscle synergies. *Curr Opin Neurobiol* **19**, 601–607.

Valero-Cuevas FJ (2015). *Fundamentals of Neuromechanics*. Springer-Verlag, London.

Valero-Cuevas FJ, Klamroth-Marganska V, Winstein CJ & Riener R (2016). Robot-assisted and conventional therapies produce distinct rehabilitative trends in stroke survivors. *J Neuroeng Rehabil* **13**, 92.

Vecchio AD, Germer CM, Elias LA, Fu Q, Fine J, Santello M & Farina D (2019). The human central nervous system transmits common synaptic inputs to distinct motor neuron pools during non-synergistic digit actions. *J Physiol* **597**, 5935–5948.

Williams ER, Soteropoulos DS & Baker SN (2010). Spinal interneuron circuits reduce approximately 10-Hz movement discontinuities by phase cancellation. *Proc Natl Acad Sci U S A* **107**, 11098–11103.

Zajac FE (1989). Muscle and tendon: Properties, models, scaling, and application to biomechanics and motor control. *Crit Rev Biomed Eng* **17**, 359–411.

Additional information

Data availability statement

The data that support the findings of this study are available from the corresponding author upon reasonable request.

Competing interests

The authors declare no competing financial interests.

Author contributions

Experiments were carried out in the laboratory of F.J.V.-C. Conception or design of the work: C.M.L., B.A.C. and F.J.V.-C.; acquisition, analysis and interpretation of data for the work: C.M.L. and B.A.C.; drafting the work: C.M.L.; revising the work critically for important intellectual content: C.M.L., B.A.C. and F.J.V.-C. All authors have read and approved the final version of this manuscript and agree to be accountable for all aspects of

the work in ensuring that questions related to the accuracy or integrity of any part of the work are appropriately investigated and resolved. All persons designated as authors qualify for authorship, and all those who qualify for authorship are listed.

Supporting information

Additional supporting information may be found online in the Supporting Information section at the end of the article.

Statistical Summary Document